Parameter estimation in the Common Reflection Surface method: The refinement step

Farid Majana, Laboratory of Computational Geophysics (LGC/UNICAMP), fmajana@numerica.com.co

Walter Mascarenhas, Federal University of Mato Grosso do Sul (UFMS) and GeoCAD, walter@geocad.com.br

Martin Tygel, Laboratory of Computational Geophysics (LGC/UNICAMP), tygel@ime.unicamp.br

Abstract

The Common Reflection Surface (CRS) method extends the well established Normal MoveOut (NMO) method, allowing the stacking process to be applied to data arranged in settings more general than the common midpoint (CMP) gathers. For that aim, the CRS method uses the general hyperbolic moveout, which depends on the classical NMO velocity and some other parameters. As in the single-parameter NMO method, the CRS parameters are estimated applying a suitable coherence analysis to the multicoverage data. The construction of simulated (stacked) zero offset (ZO) sections in the 2D situation requires three CRS parameters. This work focuses on the estimation of these three parameters. It explains how the coherence analysis is performed by most implementations of the CRS method and compares three algorithms used to refine the CRS parameters among themselves and with the traditional NMO method. These comparisons were performed using synthetic and real data.

Introduction

This work discusses the estimation of the CRS parameters for seismic imaging in the 2D situation, when the sources and receivers are located on a single seismic line. As the NMO method, the CRS method leads to simulated zero offset (ZO) sections for points of interest along the seismic line. Assuming that the seismic line is horizontal, each point of interest corresponds to a midpoint coordinate x_0 along the seismic line and both methods, NMO and CRS, create a trace for each x_0, stacking the data for each time sample t_0.

In the NMO method the stacked value corresponding to (x_0, y_0) is obtained taking into account only the traces in the CMP gather corresponding to x_0 and according to the *NMO traveltime*

$$t^2(h) = t_0^2 + \frac{4h^2}{v_{NMO}^2}\ , \qquad (1)$$

where h is the half-offset of the source-receiver pair under consideration and v_{NMO} is the *NMO-velocity* associated to the point (x_0, t_0). The parameter v_{NMO} is estimated applying a coherence (semblance) analysis to the CMP gather related to x_0. The NMO method takes some user selected time samples, which correspond to manually picked events, and interpolates the remaining samples, obtaining the v_{NMO} velocity for the whole ZO trace at x_0.

The NMO method has well known advantages: enhancement of signal to noise ratio, attenuation of undesirable events and quick and efficient implementation. However, it has two drawbacks: the coherency analysis is restricted to CMP gathers, which encompass only part of the available data and the need to manually pick the data on selected events. The CRS method does not have such drawbacks and preserves the good features of the NMO method. It applies the general hyperbolic traveltime moveout given by

$$t^2(x,h) = [t_0 + A(x - x_0)]^2 + B(x - x_0)^2 + Ch^2 \qquad (2)$$

for all the source receivers in an appropriate neighborhood of x_0 (In equation (2), x and h are the midpoint and half-offset co-ordinates of the source receiver pair for which the traveltime is computed). As a result, the CRS method makes a better use of the available data, because such neighborhoods contain much more traces than the CMP gather. Moreover, the CRS method is fully automatic and does not depend on the manual specification of NMO velocities.

The 2D hyperbolic traveltime moveout (2) depends on three parameters, as opposed to the single VNMO parameter in equation (1). It is convenient to write these three parameters as

$$A = \frac{2\sin\beta}{v_0},\quad B = \frac{4}{v_{PST}^2}\ \text{ and }\ C = \frac{4}{v_{NMO}^2}\ , \qquad (3)$$

where β is the angle between the ZO ray and the surface's normal at the central point x_0 and v_0 is the medium velocity at that point. The coefficient C equals its NMO traveltime counterpart in equation (1). The expression $B = 4/v_{PST}^2$ is analogous to the NMO-coefficient and we call v_{PST} the *post-stack velocity*. For a horizontal seismic line and a constant near surface velocity v_0, the coefficients B and C can be alternatively written as

$$B = \frac{2t_0\cos^2\beta}{v_0}K_N \text{ and } C = \frac{2t_0\cos^2\beta}{v_0}K_{NIP}, \qquad (4)$$

where K_N and K_{NIP} represent the wavefront curvatures of the normal (simply N) and normal incident point (simply NIP) waves, see Hubral (1983). The CRS method can be used under more general hypothesis than the ones assumed to get to equations (4), as described in Chira-oliva et al. (2001). However, in this work we restrict ourselves to

the particular cases in which (4) holds and treat β, K_N and K_{NIP} as the CRS parameters.

Analogously to the NMO velocity, the CRS parameters are estimated as maximizers of some coherence measure, i.e., they are found using an otimization process. In all implementations of the CRS method that we are aware of (see Birgin et al. (1999), Garabito (2001) and Mann (2002)) this optimization process is performed in two steps. The first step solves simplified problems in order to get rough estimates for the parameters. The second step refines these parameters. The first step involves global optimization and the second step uses a local optimization method. This work presents experimental results comparing the performance and accuracy of three such local optimization methods: The Nelder Mead method, the BFGS method and Newton's method.

The optimization problem

For a given point (x_0, t_0) and for fixed CRS parameters (β, K_N, K_{NIP}), the graph of the function $T(x,h) = t(x,h;\beta,K_N,K_{NIP})$ is a surface within the volume of multicoverage data points (x,h,t). If the point (x_0,t_0) pertains to a reflection event at the ZO section to be simulated and the CRS triplet (β,K_N,K_{NIP}) provides the correct coefficients of the hyperbolic traveltime (2) representation of the given event, then, according to ray theory, the graph of T is, up to second order, tangent to the event's reflection traveltime surface. As a consequence, the coherency of the data samples $u(x,h,t)$ along the graph of T, for some suitable vicinity (called *aperture*) of (x_0,t_0), should be high. The CRS parameter estimation problem is then formulated as follows:

For each midpoint and traveltime (x_0,t_0) at the ZO section to be simulated, find the CRS parameter triplet (β,K_N,K_{NIP}) for which the coherence function attains a maximum for source-receiver pairs within a given spatial aperture around x_0 and for time samples within a time window around t_0.

The objective function

In this work we consider the most popular coherence measure used in seismic processing, the *semblance* function (Neidel and Taner (1971)), and show how it can be turned into a differentiable function of the CRS parameters by interpolating the seismic data appropriately (Differentiability is important because the BFGS method and Newton's method require differentiable objective functions.)

The semblance function is given by

$$S(\beta,K_N,K_{NIP}) = \frac{\sum_{k=-w}^{k=w}\left(\sum_{i=1}^{i=n} u_i(t_i+k)\right)^2}{n\sum_{k=-w}^{k=w}\sum_{i=1}^{i=n} u_i(t_i+k)^2}, \qquad (5)$$

where $u_i(t)$ it the interpolated sample value for trace i at time sample t and

$$t_i = t_i(\beta,K_N,K_{NIP}) = t(x_i,h_i;\beta,K_N,K_{NIP}) \qquad (6)$$

is the hyperbolic travel time (2) corresponding to the ith trace midpoint x_i and half offset h_i. Notice that S is a differentiable function of the u_i and the t_i's are differentiable functions of the CRS parameters. Therefore, by the chain rule, the semblance function S will be differentiable with respect to the CRS parameters if the interpolated sample values $q_i(t)$ are differentiable with respect to t. In this case we can even compute the partial derivative of S with respect to a CRS parameter p explicitly by

$$\frac{\partial S}{\partial p} = \sum_{i=1}^{i=n} \frac{\partial S}{\partial q_i}\frac{dq_i}{dt_i}\frac{\partial t_i}{\partial p}.$$

The second derivatives are a bit more complicated but can also be evaluated explicitly.

In the experiments reported below we used simple cubic interpolations q_i in order to get a differentiable semblance function. Our interpolation has first derivatives at every t and second derivatives except for a few ts. Formally, we used the cubic function q_i such that

$$\begin{aligned} t \le t_{\min} \Rightarrow q_i(t) &= 0 \\ t \ge t_{\max} \Rightarrow q_i(t) &= 0 \\ q_i(t_{\min}+k\Delta t) &= u_{ik} \\ q_i'(t_{\min}+k\Delta t) &= \frac{u_{i(k+1)}-u_{i(k-1)}}{2\Delta t}, \end{aligned}$$

where u_{ik} is the value of the kth sample of trace i and $(t_{\min},t_{\max})$ is the time interval covered by the seismic data. In words, q_i is zero outside the time interval of interest, it interpolates the seismic data at the time samples and its derivatives at the time samples come from a centered finite differences scheme.

General estimation strategy

The CRS estimation problem is, in general, not amenable to a full three-parameter search. In realistic data sets the amount of samples is too large for a direct search. The natural approach is, then, to divide the task into simpler searches conducted on smaller data subsets. The problem is generally split into two main steps.

The initial step

The first formulation and implementation of the CRS-parameters was proposed by Müller (2002). The initial step in that formulation has three one-parameter searches. The first one, applied to the CMP gather, is similar to the search of NMO-velocities in the NMO method. However, it is carried out on every time sample of the simulated ZO section. In Müller's approach, the CMP search estimates the *combined parameter* q, which is related to the v_{NMO} and to the CRS parameters β and K_{NIP} by the formula $q = \cos^2\beta K_{NIP} = 2v_0/(t_0 v_{NMO}^2)$. In analogy to the NMO method, a stack is performed on the CMP data and the obtained section is assumed to be an approximation of a ZO section. The next two one-dimensional searches are performed in this approximated ZO section. The second search, performed within a small aperture, estimates the angle parameter β and combines it with the parameter q to produce the K_{NIP} parameter. The last search, performed

on a larger aperture, uses the estimated β and estimates the remaining parameter K_N.

Müller's strategy was extended in Mann (2002) with the inclusion of a search in Common Shot gathers to handle conflicting dips. More recently, Garabito (2001) introduced a new initial step approach. This reference implements a two-parameter simulated-annealing method applied to diffraction traveltimes, which are hyperbolic (reflection) traveltimes under the *diffraction condition* $K_N = K_{NIP}$. This search estimates β and K_{NIP}. The parameter K_N is then estimated by an additional one-dimensional search.

The refinement step

The refinement step uses local optimization schemes that take into account a larger dataset. In this work we discuss three such methods: The Nelder-Mead method, Newton's method and the BFGS method.

The Nelder Mead Method

The Nelder Method is heuristic and can be applied to any function, continuous or not. Its implementation is quite simple and it may be the method of choice for highly oscillatory objective functions, like the semblance function we consider in this work.

Newton's Method

Newton's method is classic. It has a well established convergence theory but requires objective functions with second derivatives. In order to use it we need to estimate such derivatives and manipulate the objective function's Hessian or its inverse. These Hessian computations may be costly for problems with many parameters. However, in our case we have only three parameters and our formulation of the objective function leads to efficient computation of the second derivatives. In general, Newton's method may have difficulties to handle iterations at points where the objective function's Hessian is not negative definite. Fortunately, in our particular problem we developed a simple and effective strategy to handle non negative Hessians.

The BFGS Method

The BFGS method is an adaptation of Newton's method. It does not require second derivatives or the manipulation of Hessian matrices or their inverse. It does require the first derivatives of the objective function and the manipulation of matrices that approximate the Hessian. However, in our case these derivatives are easily computed and the Hessian approximation are small matrices (3×3) and their manipulation is not expensive.

The Nelder Mead method was first used at the refinement step in the Karlsruhe's CRS (see Mann (2002)) and (Garabito (2001)) uses the BFGS refinement method. As far as we know, the present work is the first to use Newton's method for the refinement step and we intend to perform a more comprehensive comparison of such refinement methods in the future.

Experiments

To understand and compare the estimation procedures above, as well as the quality of the stacked sections they create, we applied them to synthetic and a real data. We focused on the refinement step in both cases and used the same initial estimates for all the refinement methods. The datasets were processed by the CRS method, as implemented by the program MULTISIS, which was developed by the authors at the Laboratory of Computational Geophysics at the State University of Campinas (LGC/Unicamp). MULTISIS adopts the same initial-step strategy as in Mann (2002). For comparison, we also processed the data with the NMO method as routinely carried out in the industry, with the software PROMAX of Landmark Graphics Corporation.

Synthetic data

To verify the accuracy of the parameters estimated by the methods discussed above, we generated a synthetic dataset from the velocity model shown in figure 1. The dataset and the modelled CRS parameters were obtained by the ray-tracing program SEIS88. We compared the modelled parameters with the ones estimated by the MULTISIS software, using the methods of Nelder Mead, Newton and BFGS in the refinement step.

Regarding the stacked sections, Figure 2 shows the NMO stack and the CRS initial and Newton-refined stacks. Figures 3 and 4 display the modelled, initial and optimized emergence angle over the third reflector. In figure 4 we focus on the two boxes in figure 3 and show (1) To the left, the optimization may not improve the initial value of the parameter and (2) To the right, angle values in the caustic region between CDPs 280-360.

In order to quantify the accuracy of the processed parameters, we compared their values along each reflector with the corresponding curve of the modelled parameter. The distance between the processed and computed curves was measured by the root mean distance, given by $rmd = \sqrt{(\sum_i (x_i - y_i)^2)}$, where x_i is the ith element of the modelled parameter curve and y_i is the corresponding parameter in the processed curve. Table 1 summarizes the rmd of the CRS parameters for each reflector.

Real data

An analogous treatment has been carried out on a marine dataset. Figure 5 shows the NMO stack, processed by PROMAX, and the CRS stack, obtained by MULTISIS using Newton's method in the refinement step. The CRS stacks obtained using the three refinements (Nelder Mead, Newton's and BFGS) are quite similar, and for that matter not shown. In fact, the BFGS provided a slightly smoother section, but significant to justify a discussion here.

We can verify, however, that the NMO and CRS stacks present quite a few differences. In the upper part of the sections (up to 250 ms), the NMO stack shows a better quality than its CRS counterpart. This may be due to the manual mute characteristic of the NMO processing. The automatic aperture selection of the CRS method seems not to be as

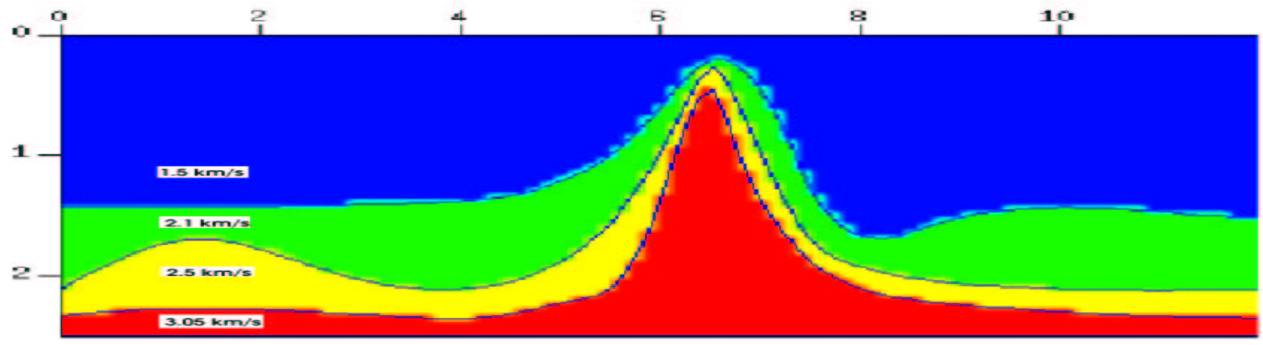

Figure 1: 2D iso-velocity layered model. Simulated multicoverage acquisition was carried out over the entire profile using 200 shot records of 60 receivers each. Horizontal distances and depths in km.

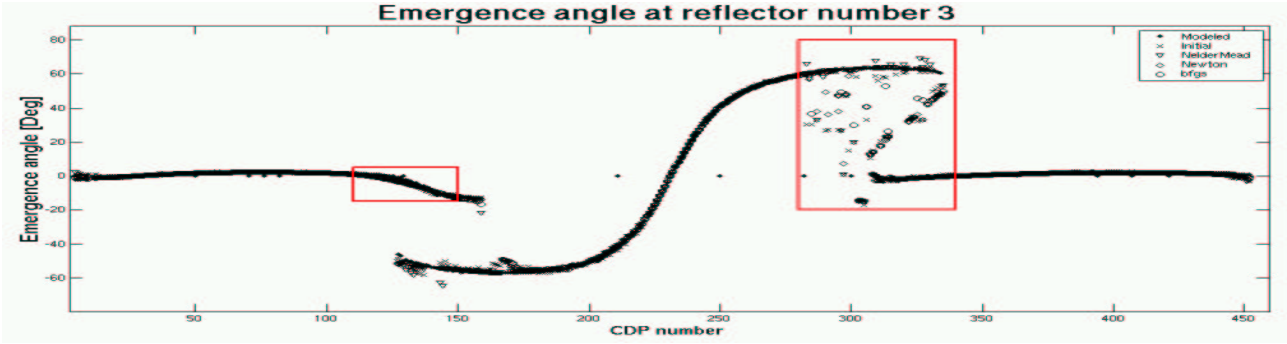

Figure 3: Modelled, initial and optimized emergence angles at the third reflector. The boxes are zoomed in Figure 4.

Angle				
reflector	**Initial**	**Nelder Mead**	**Newton**	**BFGS**
1	3.6442	4.2966	3.6528	3.6538
2	3.8321	4.1348	4.0039	3.8735
3	5.4457	4.9932	5.1889	4.8990
Knip				
reflector	**Initial**	**Nelder Mead**	**Newton**	**BFGS**
1	0.0051	0.0053	0.0050	0.0050
2	0.0090	0.0091	0.0116	0.0106
3	0.0060	0.0057	0.0053	0.0053
Kn				
reflector	**Initial**	**Nelder Mead**	**Newton**	**BFGS**
1	0.0081	0.0073	0.0068	0.0065
2	0.0145	0.0140	0.0139	0.0139
3	0.0153	0.0143	0.0136	0.0133

Table 1: Root mean distance (rmd) for CRS parameters at reflectors.

effective in this region. In the central part of the sections (between 250 ms and 1250 ms) the CRS stack presents less aleatory noise, better continuity of the primaries and less reverberations. Due to these characteristics, the CRS stack is able to better define the unconformity that occurs between 1300 ms and 1500 ms along all the section. Between the CMPs 200 and 300 and for times between 1500 ms and 1800 ms, the NMO stack has preserved diffractions that are not observed in the CRS stack. This is probably due to the fact that in the present implementation, the CRS method has considered only one attribute triplet for each time sample. In other words, possible conflicting dips were not considered. Another possibility is that the CRS method is considering too large apertures. The diffractions are being attenuated through the stack of a large number of traces where the diffractions are not present. Near the CMP 300, the CRS stack shows a horizontal event, not appearing in the NMO stack. Analysis of the CMP data (not shown here) confirms that this event actually exists. For this event, the velocity determined by the CRS method is larger than the velocities of the corresponding nearby events. This could explain why the NMO method was not able to provide a proper stack. Finally, in the lowest part of the section, between CMPs 250 and 400, the CRS stack has made more evident a probable basement structure.

It is out of the scope of the present paper, however, to undertake a detailed investigation on the NMO and CRS stacking results. Our aim here is just to point out that there are significant differences that require a better understanding and interpretation.

Conclusions

We have provided an overview of the Common-Reflection-Surface (CRS) method, encompassing a brief description of both its theoretical and implementation aspects. Our description considered the 2-D situation in which sources and

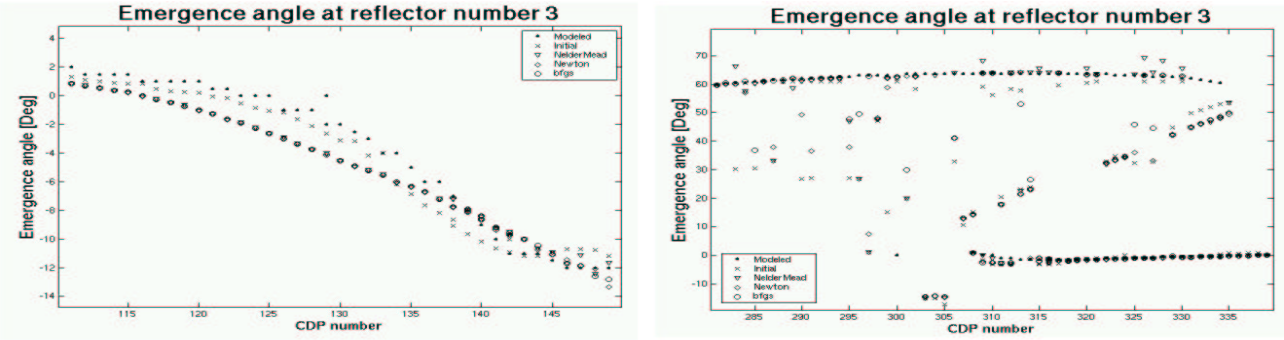

Figure 4: Zoomed boxes (caustic regions) of Figure 3. Left box (km 2.7 to km 3.7 in the velocity model). Right box (km 7.0 to km 8.5 in the velocity model). Note that initial values may be closer to modelled ones than optimized values.

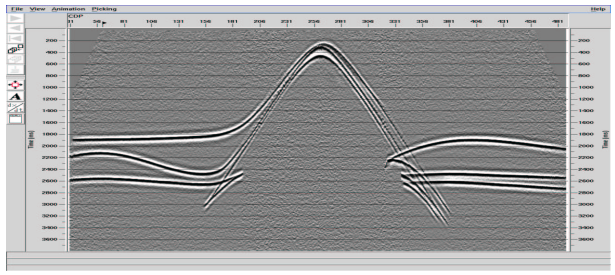

(a)

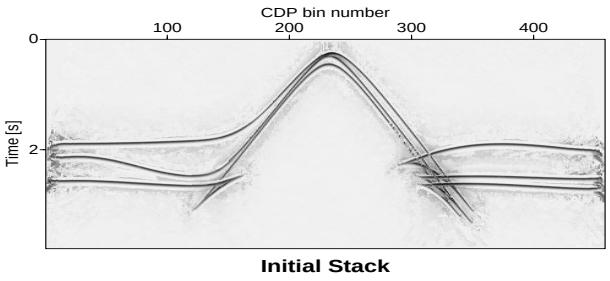

(b)

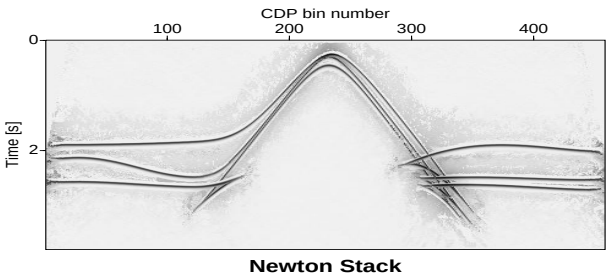

(c)

Figure 2: Synthetic stacks: (a) PROMAX; (b) Initial CRS parameters and (c) Newton optimized CRS parameters.

receivers were located on a single seismic line and that the multicoverage data is aimed in producing, by stacking, a simulated ZO section. The CRS method uses a three-parameter hyperbolic traveltime moveout. The heart of the method is the estimation of the CRS parameters. The general strategy is to split the estimation into two steps. In the first step, a quick estimation (called initial step) is performed using a suite of simplified versions of the problem. The next step (called refinement step) optimizes the parameters using the intitial estimates and the full multicoverage data. Assuming that initial estimates of the parameters were given, we examined three local optimization schemes to refine them, namely the Nelder Mead, Newton and BFGS methods. Our experiments show that the three methods lead to similar stacked sections. The CRS method, as well documented in the literature, produces, in general, sharper sections with less noise, as compared to the usually smoother NMO sections. Being a more automatic procedure, the CRS sections may, however, enhance undesirable events such as multiples.

Regarding the estimation of the CRS parameters, our experiments show that, surprisingly, the refinement step may not lead to better parameter estimates in synthetic models. Sometimes the refinement step may even lead to less accurate estimates. We do not fully understand this fact. We believe that it is caused by the lack of precision of maximizers of the semblance function as estimators for the CRS parameters. However, there may be other causes, like the failure of the optimizers to find the global maximizers. At the moment we are engaged in more experiments and research to fully understand this loss of precision in the estimates during the refinement step.

Our tests with a real dataset showed a few significant differences between the CRS and NMO stacks. These differences, briefly addressed in the text, indicate the potential of the CRS method to be used in practice. In fact, we hope that this work stimulates further investigations on the CRS method, especially on the interpretative aspects of the obtained sections.

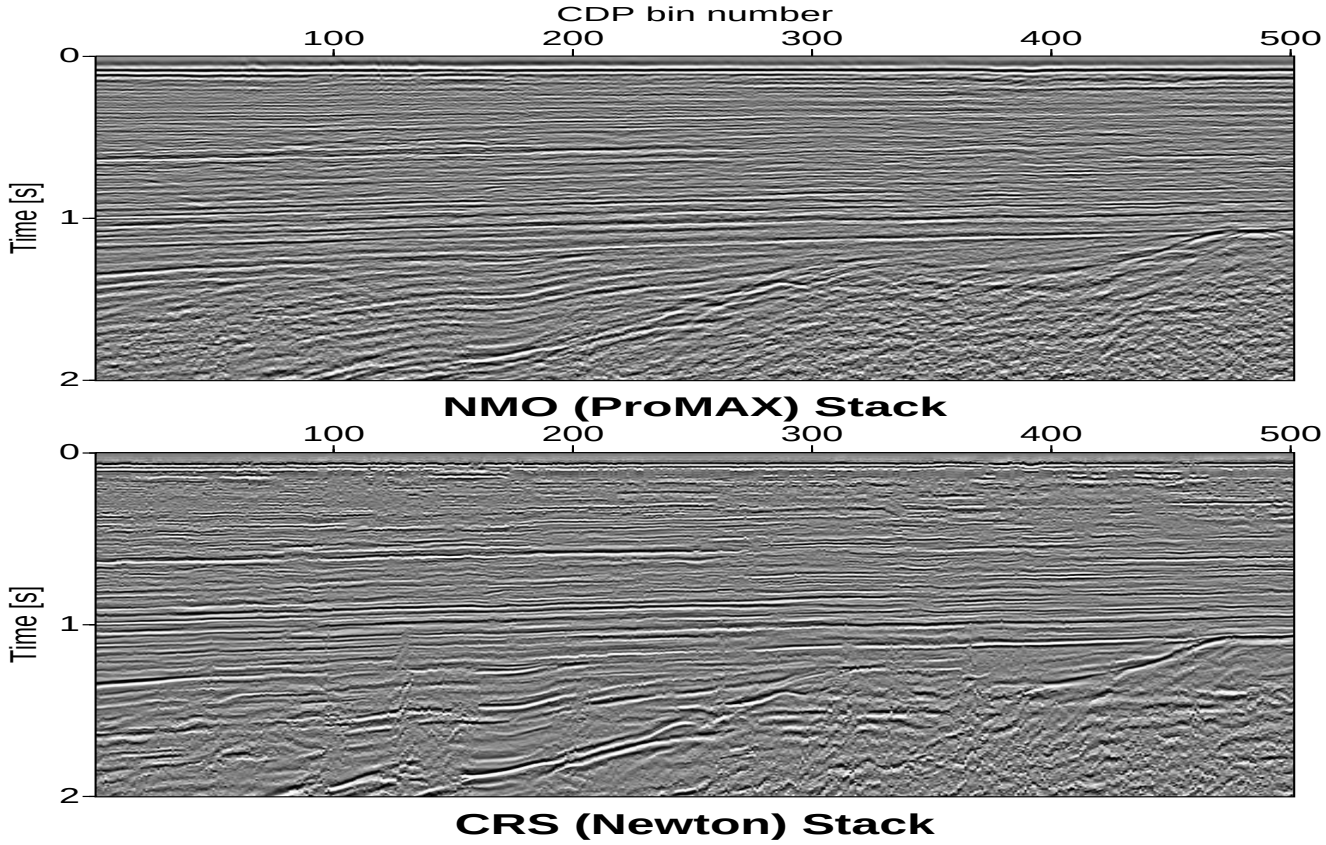

Figure 5: Marine real data stacks. Top, NMO (PROMAX) stack. Bottom, CRS (Newton) stack.

Acknowledgements

This work has been partially supported by National Council of Scientific and Technological Development (CNPq-Brazil) (grant 300927/82-7) and the Research Foundation of the State of São Paulo (FAPESP-Brazil), grant 01/01068-0). The starting point of MULTISIS was the version 4.2 of the CRS software produced in the University of Karlsruhe and described by J. Mann. We thank all support and helpful discussions concerning the CRS theory and implementation provided by P. Hubral and co-workers at the University of Karlsruhe, as well as the sponsors of the Wave Inversion Technology (WIT). Updated versions of that software have been produced in the framework of the WIT Consortium. We are thankful to the National Petroleum Agency (ANP) for permission to show the marine real dataset used in this work. We also gratefully acknowledge Landmark Graphics Corporation (Strategic University Alliance Grant no. 2002-COM-014331) for the use of PROMAXsoftware. Pictures were generated with the Seismic Unix (SU) software, release 3.5.3, provided by the Center for Wave Phenomena, Colorado School of Mines. We finally thank E. Filpo and C. Guerra (Petrobras) for helpful discussions and suggestions.

References

Birgin, E., Biloti, R., Tygel, M., and Santos, L., 1999, Restricted optimization as a clue to fast and accurate implementation of the common reflection surface stack method: J. Appl. Geoph, **42**, 143–155.

Chira-oliva, P., Tygel, M., Zhang, Y., and Hubral, P., 2001, Formula for a 2d curved measurement surface and finite-offset reflections: Journ. Seism. Explor., **10**, 245–262.

Garabito, G., 2001, Empilhamento de superfícies de reflexão comum: Uma nova seqüência de processamento usando otimização global e local: Ph.D. thesis, Universidade Federal do Pará, Brazil.

Hubral, P., 1983, Computing true amplitude reflections in a laterally inhomogeneous earth: Geohpysics, **48**, 1051–1062.

Mann, J., 2002, Extensions and application of the common reflection surface stack method: Ph.D. thesis, Universität Karlsruhe, Germany.

Müller, J., 2002, Extensions and application of the common reflection surface stack method: Ph.D. thesis, Universität Karlsruhe, Germany.

Neidel, N., and Taner, M., 1971, Semblance and other coherency measures for multichannel data: Geohpysics, **36**, 482–497.